




Article

Korean Red Ginseng Attenuates Particulate Matter-Induced Senescence of Skin Keratinocytes

Kyoung Ah Kang ^{1,2,†}, Mei Jing Piao ^{1,2,†}, Pincha Devage Sameera Madushan Fernando ¹,
Herath Mudiyansele Udari Lakmini Herath ¹, Joo Mi Yi ³ and Jin Won Hyun ^{1,2,*} 

¹ Department of Biochemistry, College of Medicine, Jeju National University, Jeju 63243, Republic of Korea; legna07@jejunu.ac.kr (K.A.K.); mjpio@jejunu.ac.kr (M.J.P.); sameera@stu.jejunu.ac.kr (P.D.S.M.F.); lakmini@stu.jejunu.ac.kr (H.M.U.L.H.)

² Jeju Research Center for Natural Medicine, Jeju National University, Jeju 63243, Republic of Korea

³ Department of Microbiology and Immunology, College of Medicine, Inje University, Busan 47392, Republic of Korea; jmyi76@inje.ac.kr

* Correspondence: jinwonh@jejunu.ac.kr; Tel.: +82-64-754-3838

† These authors contributed equally to this work.

Abstract: Skin is a direct target of fine particulate matter (PM_{2.5}), as it is constantly exposed. Herein, we investigate whether Korean red ginseng (KRG) can inhibit PM_{2.5}-induced senescence in skin keratinocytes. PM_{2.5}-treated human keratinocyte cell lines and normal human epidermal keratinocytes showed characteristics of cellular senescence, including flat and enlarged forms; however, KRG suppressed them in both cell types. Moreover, while cells exposed to PM_{2.5} showed a higher level of p16^{INK4A} expression (a senescence inducer), KRG inhibited its expression. Epigenetically, KRG decreased the expression of the ten-eleven translocation (TET) enzyme, a DNA demethylase induced by PM_{2.5}, and increased the expression of DNA methyltransferases suppressed by PM_{2.5}, resulting in the decreased methylation of the p16^{INK4A} promoter region. Additionally, KRG decreased the expression of mixed-lineage leukemia 1 (MLL1), a histone methyltransferase, and histone acetyltransferase 1 (HAT1) induced by PM_{2.5}. Contrastingly, KRG increased the expression of the enhancer of zeste homolog 2, a histone methyltransferase, and histone deacetyltransferase 1 reduced by PM_{2.5}. Furthermore, KRG decreased TET1, MLL1, and HAT1 binding to the p16^{INK4A} promoter, corresponding with the decreased mRNA expression of p16^{INK4A}. These results suggest that KRG exerts protection against the PM_{2.5}-induced senescence of skin keratinocytes via the epigenetic regulation of p16^{INK4A}.

Keywords: fine particulate matter; skin cellular senescence; Korean red ginseng; epigenetic alteration



Citation: Kang, K.A.; Piao, M.J.; Fernando, P.D.S.M.; Herath, H.M.U.L.; Yi, J.M.; Hyun, J.W. Korean Red Ginseng Attenuates Particulate Matter-Induced Senescence of Skin Keratinocytes. *Antioxidants* **2023**, *12*, 1516. <https://doi.org/10.3390/antiox12081516>

Academic Editor: Jiankang Liu

Received: 27 June 2023

Revised: 24 July 2023

Accepted: 27 July 2023

Published: 28 July 2023



Copyright: © 2023 by the authors. Licensee MDPI, Basel, Switzerland. This article is an open access article distributed under the terms and conditions of the Creative Commons Attribution (CC BY) license (<https://creativecommons.org/licenses/by/4.0/>).

1. Introduction

Air pollutants in cities represent a serious health problem, with fine particulate matter (PM_{2.5}) accounting for a large portion, owing to coal combustion and diesel exhaust fumes [1]. Both indoors and outdoors, PM_{2.5} damages several human systems, including the cardiovascular, central nervous, and pulmonary immune systems [2–5]. PM_{2.5} mainly penetrates the skin barrier via the appendix pathway and stratum corneum, which can interfere with skin protection activities, resulting in wrinkles and thickening [6,7]. Furthermore, PM_{2.5} may induce both oxidative stress and inflammation, leading to skin aging [8]. Previously, we have reported that PM_{2.5} contributes to senescence in human keratinocytes through oxidative-stress-dependent epigenetic regulation [9].

Changes in the external environment, such as exposure to PM_{2.5}, have been reported to affect gene expression through epigenetic regulation [10,11]; wherein, PM exposure leads to hypo-methylation in the promoters of genes involved in oxidative stress, inflammation, DNA repair, and cell cycle regulation.

In mammals, gene expression is strictly controlled by epigenetic modifications, such as DNA methylation and histone modifications. In general, the methylation of DNA via DNA

methyltransferases (DNMT1, DNMT3A, and DNMT3B) induces transcriptional silence. However, three DNA demethylases (ten-eleven translocations, TETs: TET1, TET2, and TET3) can reverse this methylation process, leading to transcriptional activation [12,13]. In addition to DNA methylation, many post-translation variations in histones play an essential role in changing chromatin structures and gene expression. The methylation of histone lysine and arginine residues is a marker of gene regulation. Histone methylation is complex, because residues can be mono-, di-, or trimethylated, and these indications can activate or inhibit gene transcription [14]. Di- and trimethylation of H3K4, H3K36, and H3K79 by a histone methyltransferase (HMT) are strongly correlated with the active transcription of genes, while the methylation of H3K9 and H3K27 by other HMTs inhibits transcription [15]. Furthermore, the acetylation of histone-tailed lysine residue is another marker of gene regulation. Histone acetyltransferases (HATs) add negatively charged acetyl groups to histones. This destabilizes the electrostatic interactions between the DNA surrounding the histone core, leading to transcription activation. On the contrary, acetyl group removal of histone deacetyltransferase (HDAC) regenerates stabilized electrostatic interactions, thereby inhibiting transcription induction.

Cellular senescence is typically characterized by a large, flat cell morphology, senescence-associated heterochromatin foci (SAHF), and β -galactosidase activity [16]. The tumor repressor p16^{INK4A} is a major controller of cellular senescence and inhibits cell cycle progression through its action as a specific cyclin-dependent kinase (CDK) 4 and 6 inhibitor [17]. Recently, it has been suggested that widespread epigenetic changes in senescent cells are crucial for the induction, progression, and maintenance of senescence [18]. The expression of p16^{INK4A} mRNA is reduced via the methylation of DNA at its CpG promoter site [19–21]. Moreover, in nucleosomal histones, p16^{INK4A} expression is silenced by H3K27Me3 via the enhancer of zeste homolog 2 (EZH2), an HMT [22]. In addition, p16^{INK4A} expression can be suppressed by HDAC, which binds to the p16^{INK4A} promoter and represses p16^{INK4A} transcription [23]. In contrast, mixed-lineage leukemia 1 (MLL1), an HMT, binds to the p16^{INK4A} promoter, promoting H3K4Me3 and activating p16^{INK4A} transcription during premature senescence [24]. Furthermore, HAT binds to the p16^{INK4A} promoter and induces the transcription of p16^{INK4A} [25].

Ginseng (*Panax ginseng* C. A. Meyer) is regarded as a traditional medicine and is used as a nutritional supplement and for the treatment of various diseases in Asia, such as cancers, immune disorders, and liver diseases. Recent clinical studies have shown that Korean red ginseng (KRG) normalizes various antioxidant markers to suppress intracellular oxidative stress [26]. KRG extract has also been shown to regulate nuclear factor kappa B (NF- κ B) activation, microRNA biogenesis, and the endothelial nitric oxide synthase/nitric oxide pathway, likely by stimulating the heme oxygenase/carbon monoxide pathway [27–30]. However, the epigenetic molecular mechanisms and effects of KRG on senescence in human keratinocytes remain uncertain. Therefore, herein, we have examined whether KRG could reduce the PM_{2.5}-induced senescence of human keratinocytes via epigenetic regulation.

2. Materials and Methods

2.1. Reagents

The 3-(4,5-Dimethylthiazol-2-yl)-2,5-diphenyltetrazolium bromide (MTT; cat. M5655) was obtained from Sigma-Aldrich Co., Ltd. (St. Louis, MO, USA). The primary antibodies against p16^{INK4A} (cat. #80772), DNMT3A (cat. #2160) and EZH2 (cat. #5246), were obtained from Cell Signaling Technology (Danvers, MA, USA). The TET1 (cat. MA5-16312), MLL1 (cat. A300-374A), and TATA-binding protein (TBP; cat. MA1-189) antibodies were obtained from Thermo Fisher Scientific Inc. (Waltham, MA, USA). The DNMT1 (cat. ab87654), H3K27Me3 (cat. ab195477), and H3K4Me3 (cat. ab8580) antibodies were obtained from Abcam (Cambridge, UK). The TET2 (cat. sc-398535), TET3 (cat. sc-518126), DNMT3B (cat. sc-376043), and actin (cat. sc-47778) antibodies were obtained from Santa Cruz Biotechnology (Santa Cruz, CA, USA). The SPiDER- β Gal kit was obtained from Dojindo Molecular Technologies (Rockville, MD, USA).

2.2. KRG Preparation

The KRG was prepared by the Korea Ginseng Corporation (Seoul, Republic of Korea) from the roots of 6-year-old *P. ginseng* plants, as described previously [31]. Subsequently, *P. ginseng* was steamed for 3 h at 90–100 °C, after which it was dried at 50–80 °C. The KRG was then extracted through water circulation for 8 h at 85–90 °C. The ginsenosides of KRG were compared to the ginsenoside standards using ultra-performance liquid chromatography. The prepared KRG mainly contained the following ginsenosides: Rb1 (4.62 mg/g), Rg2 (3.21 mg/g), Rg3 (3.05 mg/g), Rc (2.41 mg/g), Rb2 (1.83 mg/g), Rf (1.21 mg/g), Rd (0.89 mg/g), Re (0.93 mg/g), and Rg1 (0.71 mg/g). The KRG was dissolved in dimethyl sulfoxide (DMSO) with final DMSO concentrations of <0.1% treated into the cell medium.

2.3. PM_{2.5} Preparation

Standard diesel PM (SRM 1650b, Sigma-Aldrich Co., Ltd.), with an average diameter of 0.18 µm, was used, mostly comprising polycyclic aromatic hydrocarbons (PAHs) and nitro-PAHs. Information on nitro-PAHs and PAHs in SRM 1650b, such as the certified mass fraction values, can be found in previously published papers [32,33]. PM_{2.5} in DMSO was prepared for stock, with DMSO as the control and with concentrations not exceeding 0.01%.

2.4. Keratinocyte Culture

The human keratinocytes cell line HaCaT was obtained from the CLS Cell Lines Service (Eppelheim, Germany). Normal human epidermal keratinocytes (NHEK) were obtained from Thermo Fisher Scientific. The HaCaT cells were seeded using a complete DMEM medium with 10% fetal bovine serum and 1% antibiotics. NHEK cells were cultured using EpiLife serum-free medium with added EpiLife undefined growth supplements (Thermo Fisher Scientific). All cells were incubated at 37 °C in a 5% CO₂ incubator.

2.5. Cell Viability

To detect the cytotoxicity effect of KRG, cells were seeded (1×10^5 cells/mL) and treated with 2, 4, 6, 8, 10, 20, 40, 80, or 100 µg/mL of KRG. After 48 h, the cells were cocultured with MTT solution. After a four-hour-long incubation period, the transformed formazan crystals were dissolved in DMSO. The formazan product was measured at an absorbance of 540 nm under a scanning multi-well spectrophotometer (Thermo Fisher Scientific).

2.6. Detection of Intracellular Reactive Oxygen Species (ROS)

To measure the ROS scavenging effect of KRG, we proceeded with 2',7'-dichlorofluorescein diacetate (DCF-DA; Sigma-Aldrich Co., Ltd.) staining. The cells were pre-treated with 2, 4, 6, 8, 10, or 20 µg/mL of KRG and then treated with PM_{2.5} (50 µg/mL) for 24 h, which generated ROS, followed by the addition of 25 µM of DCF-DA. The ROS levels were detected using flow cytometry (Becton Dickinson, Mountain View, CA, USA) [34].

2.7. Colony Formation Detection

To detect the colony-forming ability (CFA), cells were seeded to 5×10^2 cells/mL in a 60-mm dish. The colony expansion of single cells was allowed to progress for 3 days, after which they were pre-treated with 20 µg/mL of KRG, and then 50 µg/mL of PM_{2.5} was added for 7 days. The colony formation detection was performed using a Diff-Quik kit (Sysmex Corporation, Kobe, Japan). The Diff-Quik staining solution was used to stain the resulting colonies after fixing with Diff-Quik fixation solution.

2.8. SAHF Detection

To measure SAHF, an indicator of cellular senescence, cells were seeded to 1.0×10^5 cells/mL on microscope slides, pre-treated with 20 µg/mL of KRG, and then treated with PM_{2.5} (50 µg/mL) for 24 h. Subsequently, the cells were labeled on the nu-

cleus by 4',6-diamidino-2-phenylindole (DAPI) staining. Cells were imaged using a Zeiss confocal microscope and LSM 510 software version 4.2 (Carl Zeiss, Oberkochen, Germany).

2.9. Immunofluorescence

To measure the expression of epigenetic-related proteins, the cells were seeded to 1.0×10^5 cells/mL on microscope slides, were pre-treated with 20 $\mu\text{g}/\text{mL}$ of KRG, and then treated with $\text{PM}_{2.5}$ (50 $\mu\text{g}/\text{mL}$) for 24 h. Subsequently, the cells were fixed with 4% paraformaldehyde for 15 min and permeabilized with a permeable reagent (phosphate-buffered saline, PBS, containing 0.1% Triton X-100) for 15 min. The cells were incubated with a blocking solution (PBS containing 3% BSA) for 1 h and then incubated with the primary antibody diluted in the blocking solution for 2 h. The secondary antibody was incubated for 1 h using Alexa488-binding secondary antibody (Santa Cruz Biotechnology). The cells were observed under a confocal microscope (Zeiss, LSM 510 software) after mounting with a DAPI-containing mounting medium.

2.10. β -Galactosidase Activity Detection

To measure β -galactosidase activity, an indicator of cellular senescence, the cells were seeded on microscope slides, pre-treated with 20 $\mu\text{g}/\text{mL}$ of KRG, and then treated with $\text{PM}_{2.5}$ (50 $\mu\text{g}/\text{mL}$) for 24 h. Subsequently, the cells were stained with SPiDER- β Gal staining and then incubated at 37 °C for 15 min. After that, the cells were mounted using DAPI-containing mounting medium and images were captured using a confocal microscope.

2.11. Western Blot Analysis

The cells were seeded to 1.0×10^5 cells/mL on a 60-mm culture dish. They were pre-treated with 20 $\mu\text{g}/\text{mL}$ of KRG and then treated with $\text{PM}_{2.5}$ (50 $\mu\text{g}/\text{mL}$) for 24 h. The cells were collected, and the proteins were extracted by lysis. Subsequently, the lysates of cells (60 μg of protein) were separated via 6, 10, or 12% SDS-polyacrylamide gel electrophoresis and then transferred into the membrane, which was immunoblotted with specific primary antibodies. The following primary antibodies were used; p16^{INK4A}, DNMT1, DNMT3A, DNMT3B, TET1, TET2, TET3, EZH2, H3K27Me3, MLL1, H3K4Me3, HDAC1, and HAT1. In addition, primary antibodies against actin and TBP were used as a loading control. Membranes bound with primary antibodies were contacted with secondary antibodies (Pierce, Rockland, IL, USA), and bands of protein were assessed using a western blotting detection kit (Amersham, Little Chalfont, Buckinghamshire, UK).

2.12. Quantitative Reverse Transcription Polymerase Chain Reaction (qRT-PCR)

The cells were seeded to 1.0×10^5 cells/mL on a 60-mm culture dish. They were pre-treated with 20 $\mu\text{g}/\text{mL}$ of KRG and then treated with $\text{PM}_{2.5}$ (50 $\mu\text{g}/\text{mL}$) for 24 h. For the real-time qRT-PCR, the qRT-PCR reaction system contained 5.0 μL of 2 \times SYBR Green Mixture, forward primer (5 μM), and reverse primer (5 μM) each, 1.0 μL of cDNA, and double-distilled water. The qRT-PCR conditions were as follows: pre-denatured for 10 min at 95 °C; 40 cycles at 95 °C for 15 s; and at 60 °C for 1 min on a Bio-Rad iQ5 Real-Time PCR Detection System (Bio-Rad Laboratories, Hercules, CA, USA). The qRT-PCR primers used were as follows: forward primer 5'-CTCGTGCTGATGCTACTGAGGA-3' and reverse primer 5'-GGTCGGCGCAGTTGGGCTCC-3' for the amplification of p16^{INK4A} and forward primer 5'-CACCTTCTACAATGAGCTGCGTGT-3' and reverse primer 5'-CACAGCCTGGATAGCAACGTACA-3' for actin. A prepared 1% agarose gel with ethidium bromide was used to resolve the amplification, and it was photographed under ultraviolet light using Image Quant™ TL analysis software version 10.1 (Amersham Bioscience, Uppsala, Sweden).

2.13. Quantitative Methylation-Specific PCR (qMSP) and Bisulfite Sequencing

To measure the methylation of the p16^{INK4A} promoter, a specific methylation kit (Zymo Research, Tustin, CA, USA) was used for DNA (1 μg) conversion, which involves

the chemical bisulfite conversion of unmethylated cytosine to uracil and the protection of methylated cytosine. For qMSP detection, qMSP primer pairs were used to assess gene promoter methylation sites, which are located close to the putative transcription start site of the 5' CpG islands. The qMSP was carried out using bisulfite-treated samples, was normalized based on Alu element amplification, and was assessed using the CFX96™ real-time system (Bio-Rad Laboratories). In addition, for bisulfite sequencing, bisulfite-treated DNA and JumpStart REDTaq DNA polymerase (Sigma-Aldrich Co., Ltd.) were used for the template and amplification, respectively. A gel extraction kit (Qiagen GmbH, Hilden, Germany) and clones using the TOPO TA vector system (Invitrogen, Carlsbad, CA, USA) were used to purify the PCR products in bisulfite sequencing. Then, a NucleoSpin plasmid isolation kit (Macherey-Nagel, Düren, Germany) was used for the isolation and purification of each clone. An M13F primer was used to sequence the randomly selected positive clones. After that, the methylation status of each CpG dinucleotide was examined. qMSP and bisulfite sequencing primers were obtained based on previous reports [9,35,36].

2.14. Chromatin Immunoprecipitation (ChIP) Assay

To measure the binding of epigenetic-related proteins to the p16^{INK4A} locus, the cells were pre-treated with 20 µg/mL of KRG and then treated with PM_{2.5} (50 µg/mL) for 24 h. Antibodies against TET1, DNMT1, EZH2, MLL1, HDAC1, HAT1, and normal rabbit immunoglobulin G (IgG) were used for ChIP assays, which were assessed using a SimpleChIP® enzymatic ChIP kit (Cell Signaling Technology). DNA (200 ng) recovered from the immunoprecipitated complexes was subjected to qPCR. Primers for the p16^{INK4A} locus have been described previously [9]. The forward primer used was 5'-CCCCTTGCCTGGAAAGATAC-3' and the reverse primer was 5'-AGCCCCTCCTCTTTCTTCCT-3'.

2.15. Transfection of Small Interfering RNA (siRNA)

Control siRNA (SS-1001), siRNA, TET1#1 sense (5'-CAGUGUAACCAGCACAGUU-3') and antisense (5'-AACUGUGCUGGUUACACUG-3') siRNAs, MLL1#1 sense (5'-GUCACA GUAGGUGAUCCUU-3') and antisense (5'-AAGGAUCACCUACUGUGAC-3') siRNAs, MLL1#2 sense (5'-CUAUUCUCGGGUCAUCAAU-3') and antisense (5'-AUUGAUGACCC GAGAAUAG-3') siRNAs, and HAT1#1 sense (5'-CUAUUCUCGGGUCAUCAAU-3') and antisense (5'-AUUGAUGACCCGAGAAUAG-3') siRNAs were obtained from Bioneer Corporation (Daejeon, Republic of Korea). TET1#2 (AM16708-ID:147892) and HAT1#2 (AM16708-ID:13322) siRNAs were obtained from Invitrogen. The cells were transfected using serum-free Opti-MEM containing Lipofectamine RNAiMax reagent (Invitrogen). Subsequently, we added 4 µL of Lipofectamine to 2 mL of Opti-MEM and let the mixture settle at 18–20 °C for 5 min. The siRNA was then added to the Opti-MEM-lipofectamine solution at a final concentration of 20 nM, after which the mixture was kept at 18–20 °C for 5 min. The transfection incubation was conducted for 24 h.

2.16. Statistical Analysis

Each experiment was repeated three times, and the results are indicated as the mean ± standard error of the mean (SEM). For the statistical analysis, SigmaStat software v12 (SPSS, Chicago, IL, USA) was used. One-way analysis of variance (ANOVA) and Tukey's post hoc test were used to assess the results. At $p < 0.05$, differences were considered statistically significant.

3. Results

3.1. KRG Decreased ROS Generation Induced by PM_{2.5}

Previously, we have demonstrated that 50 µg/mL of PM_{2.5} exhibited ROS-induced senescence [9]; therefore, the optimal concentration of PM_{2.5} to include cellular senescence was set as 50 µg/mL. We first estimated the cell viability at various concentrations of KRG by using HaCaT and NHEK cells, finding that KRG showed no cytotoxicity up to doses of

20 $\mu\text{g}/\text{mL}$ (Figure 1a). The ROS scavenging effect of KRG on ROS generation induced by $\text{PM}_{2.5}$ in HaCaT and NHEK cells was highest at 20 $\mu\text{g}/\text{mL}$ of KRG (Figure 1b). Therefore, 20 $\mu\text{g}/\text{mL}$ of KRG was used as the optimal concentration for the subsequent analyses.

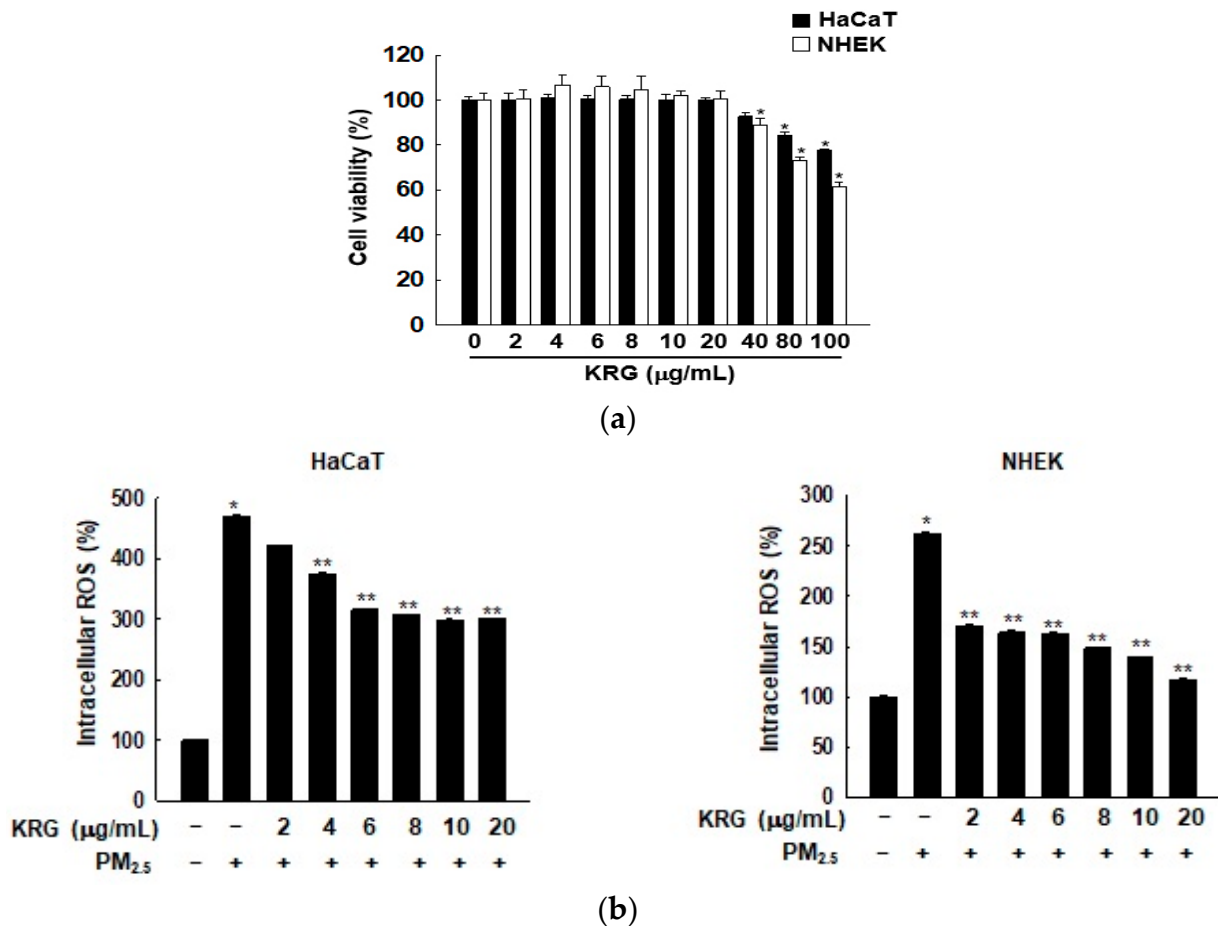


Figure 1. Scavenging effect of Korean red ginseng (KRG) against reactive oxygen species (ROS) generated by $\text{PM}_{2.5}$. (a) Cell viability after treatment with indicated concentrations of KRG in HaCaT and normal human epidermal keratinocyte (NHEK) cells was assessed. (b) Intracellular ROS were measured by flow cytometry. * $p < 0.05$ indicates significant differences with untreated cells and ** $p < 0.05$ indicates significant differences with $\text{PM}_{2.5}$ -treated cells.

3.2. KRG Attenuated Cellular Senescence Induced by $\text{PM}_{2.5}$

Oxidative stress induced by $\text{PM}_{2.5}$ significantly showed senescence phenotypes in cells, such as an irregular size, a flattened and enlarged cell shape (Figure 2a), reduced CFA (Figure 2b), increased SAHF in the nucleus (Figure 2c), and higher cytoplasmic β -galactosidase activity (Figure 2d). However, the KRG treatment nearly restored the normal cell shape (Figure 2a), increased the CFA (Figure 2b), decreased the SAHF (Figure 2c), and reduced the β -galactosidase activity (Figure 2d). The expression of the $\text{p}16^{\text{INK}4\text{A}}$ protein, a well-known CDK inhibitor and senescence inducer, was strongly induced in the $\text{PM}_{2.5}$ -treated cells, compared with that in the control cells; however, KRG treatment reduced its expression in both of the cell types (Figure 2e). In agreement with the western blotting results, $\text{p}16^{\text{INK}4\text{A}}$ mRNA in the $\text{PM}_{2.5}$ -treated cells was also induced, compared with that in the control cells; however, KRG application reduced $\text{p}16^{\text{INK}4\text{A}}$ mRNA (Figure 2f).

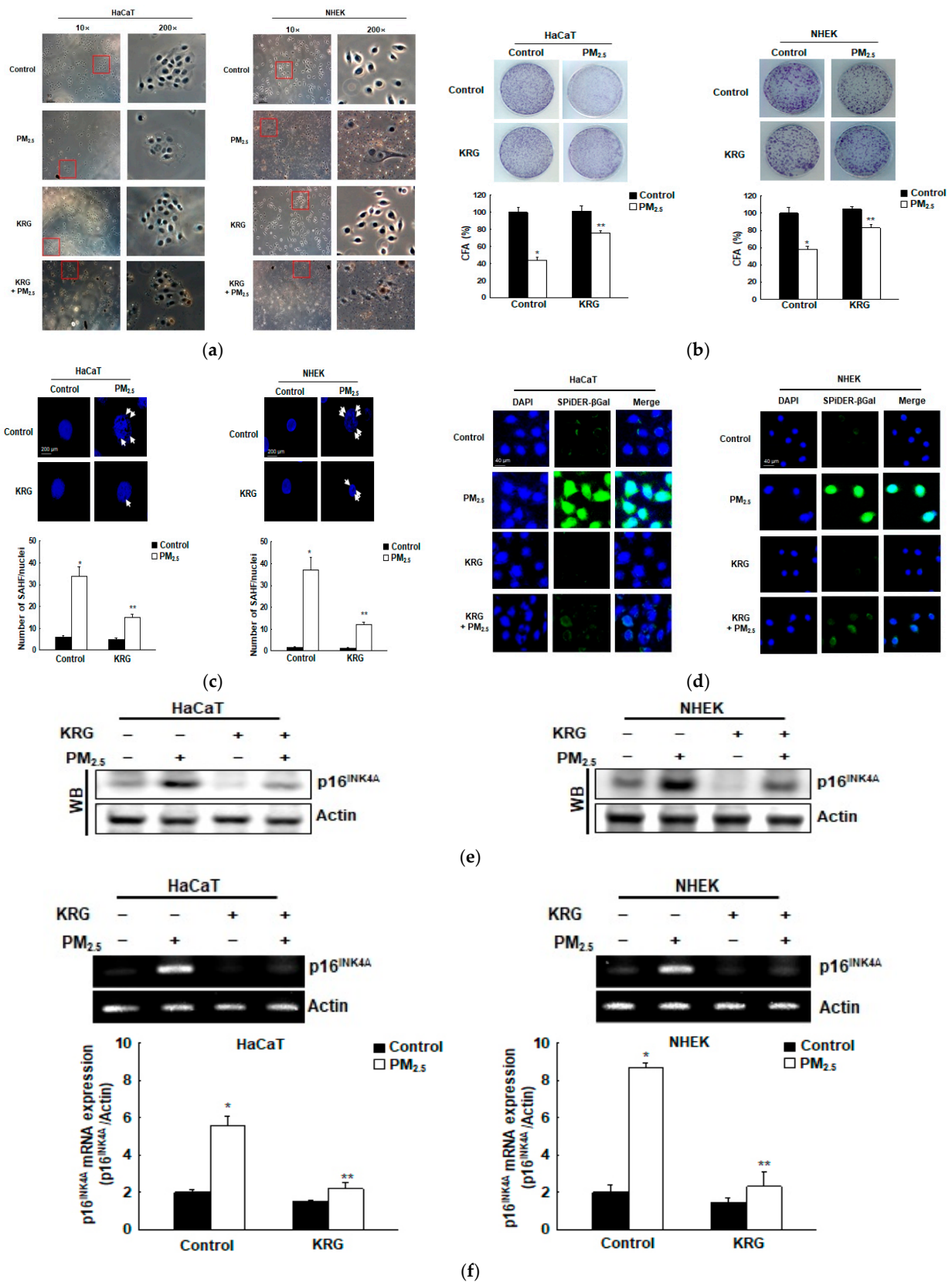


Figure 2. Inhibitory effect of KRG against cellular senescence induced by PM_{2.5}. (a) Microscopic assessment reveals that PM_{2.5} induces morphological alterations typical of cellular senescence. Red square area means enlarged cell morphology. (b) Colony-forming ability (CFA) was enumerated after Diff-Quik staining. (c) Senescence-associated heterochromatin foci (SAHF) structure after cell staining

with 4',6-diamidino-2-phenylindole (DAPI) fluorescent dye was assessed. The arrows indicate SAHF in senescent cells induced by PM_{2.5}. * $p < 0.05$ and ** $p < 0.05$ indicate significant differences with control cells and PM_{2.5}-exposed cells, respectively. (d) β -galactosidase activity was revealed by staining with DAPI (blue) and the SPiDER- β Gal (green) working solution. (e) Senescence marker p16^{INK4A} was detected by western blotting using the corresponding antibodies after cell lysates were electrophoresed. Actin represents a loading control. (f) Expression of p16^{INK4A} mRNA was assessed by qRT-PCR. * $p < 0.05$ and ** $p < 0.05$ indicate significant differences with control cells and PM_{2.5}-exposed cells, respectively.

3.3. p16^{INK4A} Expression in KRG-Treated Cells Was Attenuated through Decreased DNA Demethylation in Cellular Senescence Induced by PM_{2.5}

Our previous study demonstrated that p16^{INK4A} is epigenetically controlled via the methylation of DNA during cellular senescence induced by PM_{2.5} [9]. To determine whether KRG is involved in the regulation of PM_{2.5}-induced p16^{INK4A} transcription via epigenetic DNA methylation, we measured the p16^{INK4A} promoter methylation status using qMSP and bisulfite sequencing analysis. The DNA methylation level of the p16^{INK4A} promoter region (from -150 to +200 bp, including 35 CpG sites in the promoter of p16^{INK4A}) significantly declined in the PM_{2.5}-treated cells compared with that in the control cells; however, KRG increased the DNA methylation level in both of the cell types (Figure 3a). Subsequently, the DNA methylation status of the p16^{INK4A} locus was examined with bisulfite sequencing, revealing that the PM_{2.5}-treated cells had lower methylation levels than those of the control cells. However, KRG increased methylation in both of the cell types (Figure 3b). Therefore, KRG reduced the transcription of p16^{INK4A} in the PM_{2.5}-treated cells by attenuating epigenetic promoter methylation. In addition, western blot analyses showed that DNMT1, DNMT3A, and DNMT3B expression decreased in the PM_{2.5}-treated cells but was increased by KRG (Figure 3c). Conversely, TET1, TET2, and TET3 expression increased in the PM_{2.5}-treated cells but was reduced after applying the KRG treatment (Figure 3c). The expression of DNMTs and TETs by western blot analysis was confirmed using immunofluorescence (Figure 3d,e). We then assessed whether DNMT and TET could directly bind to the p16^{INK4A} promoter region in both cell types by employing ChIP-qPCR analysis. The binding of DNMT1 to the p16^{INK4A} promoter region decreased in the PM_{2.5}-treated cells; however, KRG increased its binding in both cell types, which showed a similar pattern to that of protein expression (Figure 3f). The binding of TET1 to the p16^{INK4A} locus increased in the PM_{2.5}-treated cells but was decreased in both cell types by KRG (Figure 3g). Furthermore, TET1 siRNA decreased the expression of p16^{INK4A} mRNA in the PM_{2.5}-treated cells, while KRG decreased PM_{2.5}-induced p16^{INK4A} expression (Figure 3h). These results indicate that PM_{2.5}-induced p16^{INK4A} expression involves the release of DNMT and the recruitment of TET participating in senescence induction. However, KRG attenuates these effects, leading to the inhibition of PM_{2.5}-induced senescence-related gene transcription.

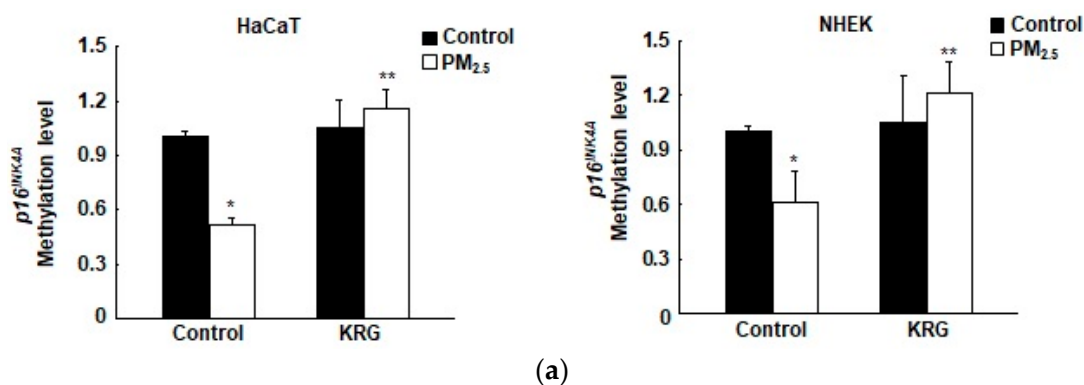


Figure 3. Cont.

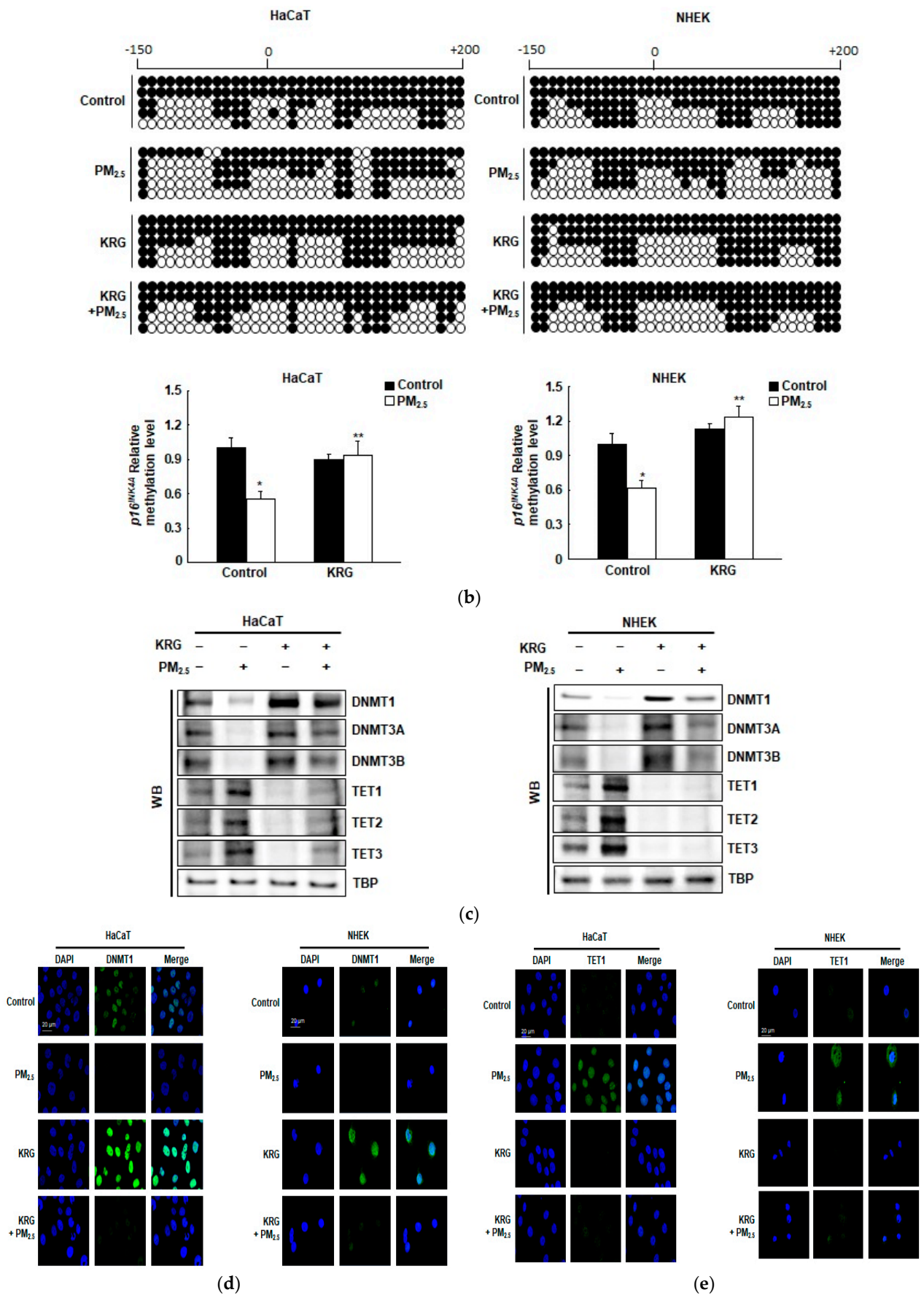


Figure 3. Cont.

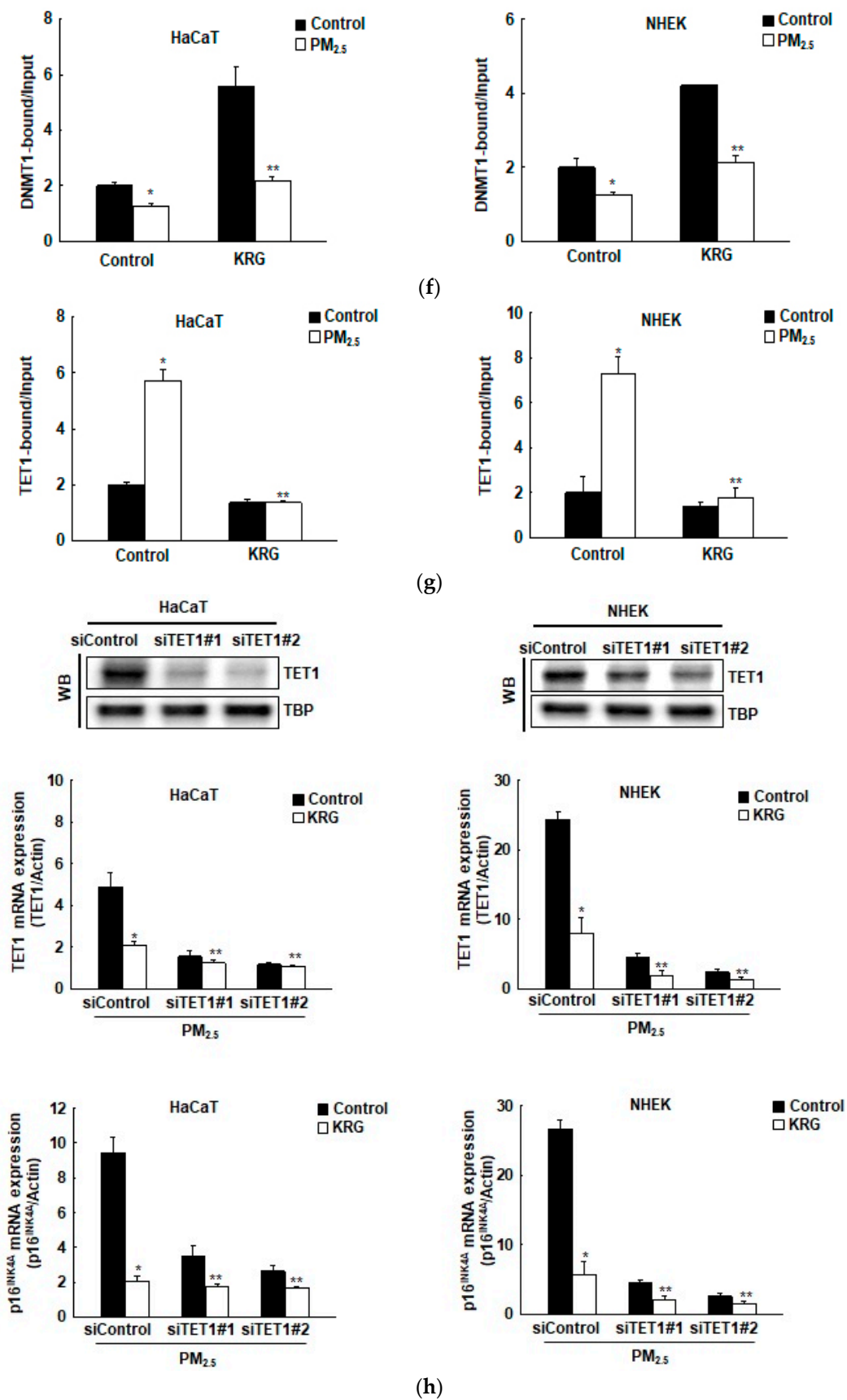


Figure 3. Attenuation of p16^{INK4A} expression in KRG-treated cells via an increase in DNA methylation. (a) The Alu element was used to normalize the quantitative methylation levels of the p16^{INK4A}

promoter region. (b) Analysis of the $p16^{INK4A}$ promoter region was assessed using bisulfite sequencing. Methylated cytosine is shown in black, whereas unmethylated cytosine is shown with white circles. The $p16^{INK4A}$ locus-targeted (chromatin immunoprecipitation (ChIP)-qPCR was carried out with the use of specified primer sets. (c) Electrophoresis of nuclear fractions was used to detect DNA methyltransferases (DNMTs) and ten-eleven translocations (TETs) via western blotting using specific antibodies. The loading control is represented here by the TATA-binding protein (TBP). (d,e) The nuclear location of (d) DNMT1 and (e) TET1 was determined by confocal microscopy after Alexa488-labeling (green) with the corresponding antibodies and staining with DAPI (blue). (f,g) ChIP assays using antibodies against (f) DNMT1 and (g) TET1 were performed and analyzed by qPCR. TET1 small interfering RNA (siRNA) was transfected into cells and then incubated for 24 h. (h) TET1 and $p16^{INK4A}$ were detected by qRT-PCR. * $p < 0.05$ and ** $p < 0.05$ indicate significant differences with control cells and $PM_{2.5}$ -treated cells, respectively.

3.4. $p16^{INK4A}$ Expression in KRG-Treated Cells Was Attenuated via Changes in Histone Methylation in Cellular Senescence Induced by $PM_{2.5}$

Our previous study demonstrated that histone methylation plays an important role in $p16^{INK4A}$ epigenetic regulation [9]. To determine whether KRG is involved in epigenetic histone methylation of $p16^{INK4A}$ expression induced by $PM_{2.5}$, we detected the expression of HMT proteins using western blot analysis. EZH2, a transcriptional suppressor and a polycomb complex component with H3K27 methyltransferase activity, and its target protein, H3K27Me3, decreased after $PM_{2.5}$ treatment; however, they were increased by KRG (Figure 4a). The expression of MLL1, a transcriptional activator with H3K4 methyltransferase activity, and its target protein (H3K4Me3) increased after $PM_{2.5}$ treatment; however, they were decreased by KRG (Figure 4a). The expressions of EZH2 and MLL1 were confirmed by immunofluorescence analysis (Figure 4b,c). We assessed whether histone methyltransferase-related proteins could directly bind to the $p16^{INK4A}$ locus in HaCaT and NHEK cells using ChIP-qPCR analysis. The binding of EZH2 to the $p16^{INK4A}$ locus was decreased in $PM_{2.5}$ -treated cells; however, KRG increased their binding, which showed a similar pattern to that of protein expression (Figure 4d). The binding of MLL1 to the $p16^{INK4A}$ locus increased in the $PM_{2.5}$ -treated cells but was decreased by KRG in both of the cell types (Figure 4e). In addition, MLL1 siRNA decreased the expression of $p16^{INK4A}$ mRNA in the $PM_{2.5}$ -treated cells, and KRG decreased the $PM_{2.5}$ -induced $p16^{INK4A}$ expression (Figure 4f). Collectively, these results indicate that the $PM_{2.5}$ -induced expression of $p16^{INK4A}$ involves the recruitment of MLL1, whereas the release of EZH2 is linked to senescence induction. However, KRG attenuates these effects, leading to the inhibition of $p16^{INK4A}$ transcription induced by $PM_{2.5}$.

3.5. $p16^{INK4A}$ Expression in KRG-Treated Cells Was Attenuated via Changes in Histone Acetylation and Deacetylation in Cellular Senescence Induced by $PM_{2.5}$

Many studies have shown that histone acetylation plays an important role in $p16^{INK4A}$ epigenetic regulation [25]. To determine whether KRG is involved in the epigenetic histone acetylation of $p16^{INK4A}$ expression induced by $PM_{2.5}$, we detected the expression of histone acetylation and deacetylation proteins using western blot analyses. The expression of the transcriptional repressor HDAC1 decreased in the $PM_{2.5}$ -treated cells with deacetylase activity; however, it was increased by KRG (Figure 5a). The transcriptional activator HAT1 increased in the $PM_{2.5}$ -treated cells with acetyltransferase activity; however, treatment with KRG decreased it (Figure 5a). The expressions of HDAC1 and HAT1 were confirmed using immunofluorescence (Figure 5b,c). Furthermore, we assessed whether histone acetyl-related proteins could directly bind to the $p16^{INK4A}$ locus using ChIP-qPCR analysis. The binding of HDAC1 to the $p16^{INK4A}$ locus was decreased in the $PM_{2.5}$ -treated cells but was increased by KRG in both cell types, with a pattern comparable to that of protein expression (Figure 5d). The binding of HAT1 to the $p16^{INK4A}$ locus increased in the $PM_{2.5}$ -treated cells but was decreased by KRG in both cell types (Figure 5e). In addition, HAT1 siRNA decreased the expression of $p16^{INK4A}$ mRNA in the $PM_{2.5}$ -treated cells, while KRG

decreased the PM_{2.5}-induced p16^{INK4A} expression (Figure 5f). Collectively, these results indicate that p16^{INK4A} expression induced by PM_{2.5} involves the recruitment of HAT1, while the release of HDAC1 is associated with cellular senescence induction. However, KRG has been shown to weaken this effect and induce the inhibition of p16^{INK4A} transcription through increased histone deacetylation.

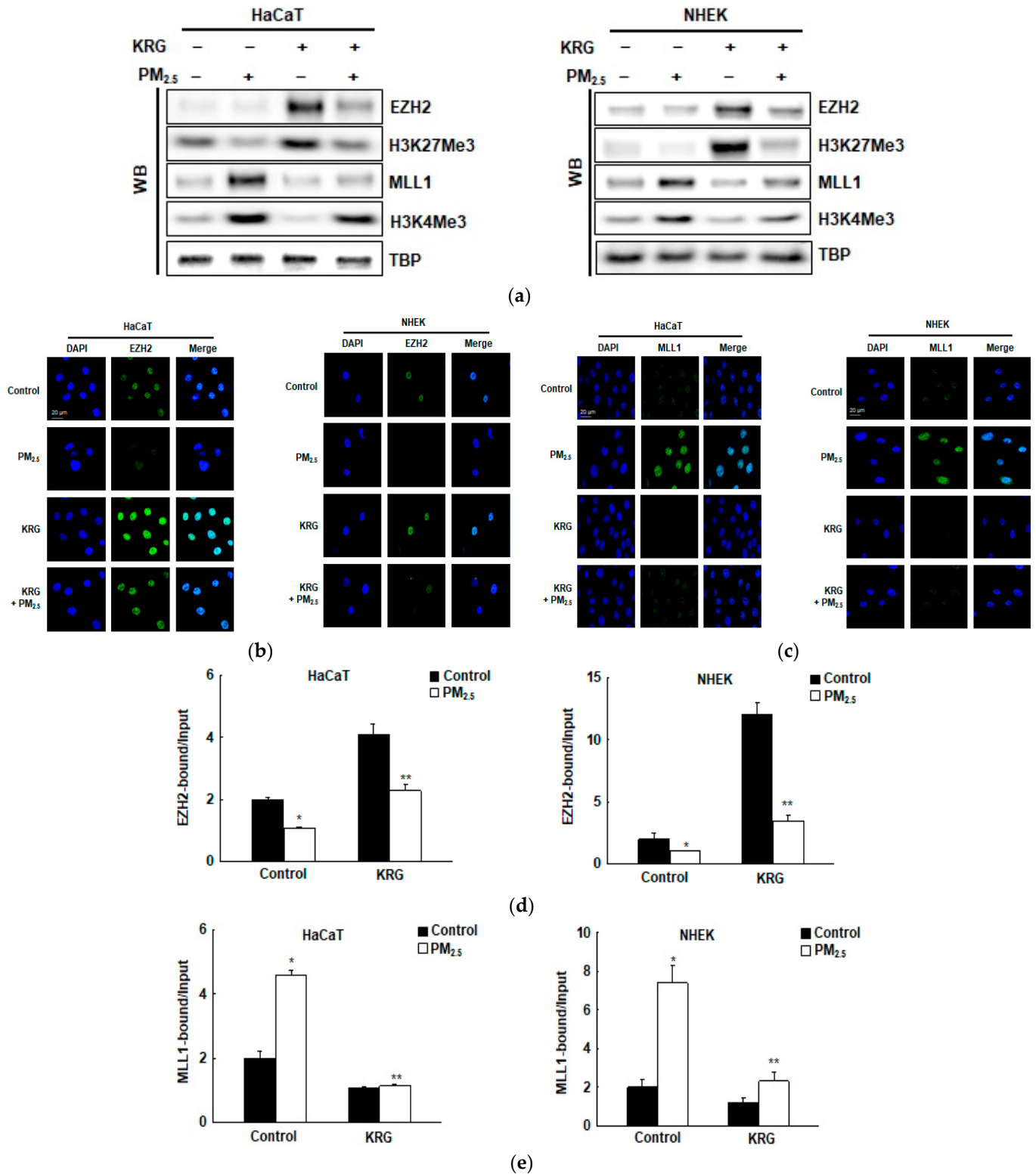


Figure 4. Cont.

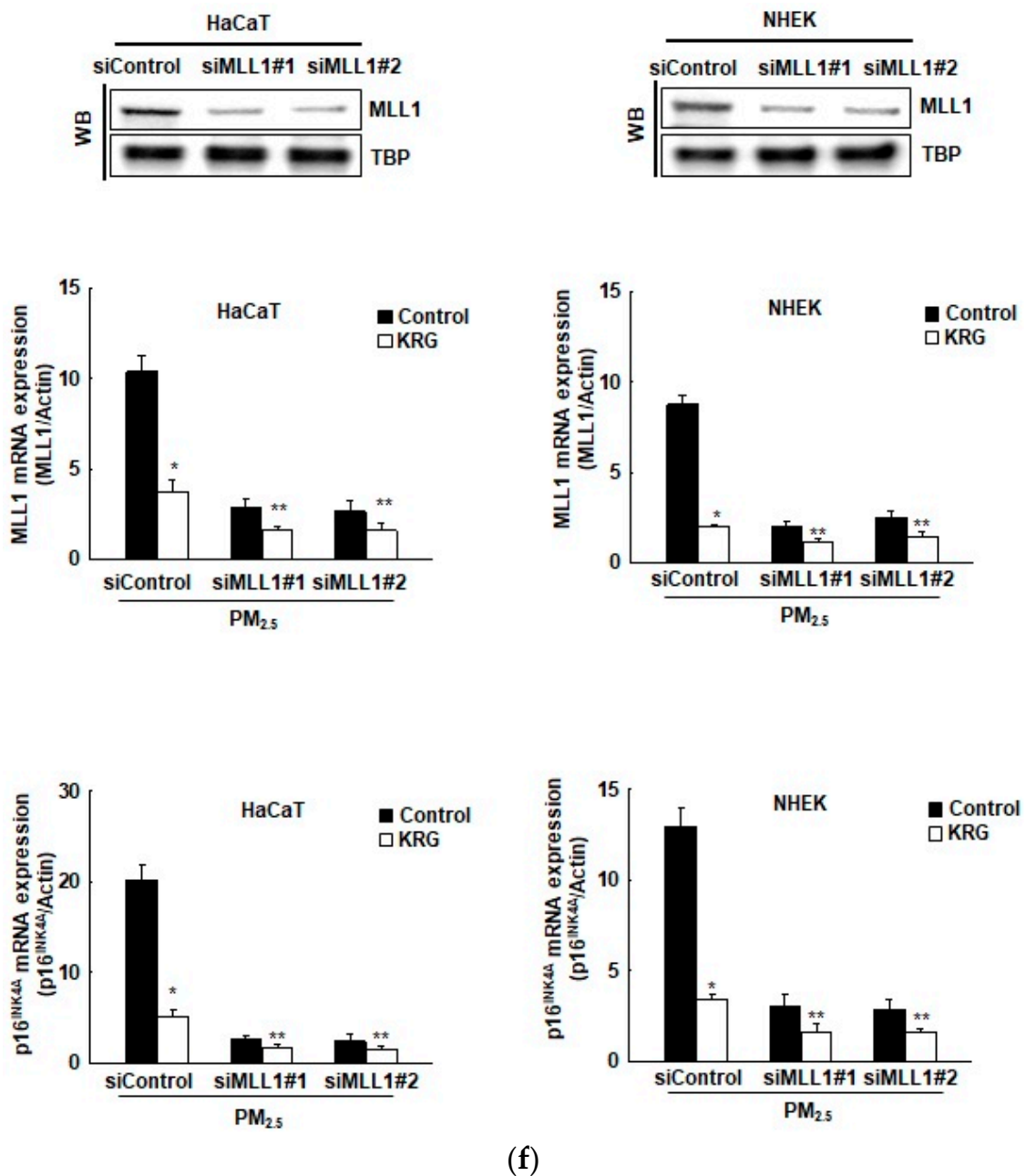


Figure 4. Attenuation of p16^{INK4A} expression in KRG-treated cells via changes in histone methylation. (a) Nuclear fractions were electrophoresed, and enhancers of zeste homolog 2 (EZH2), H3K27Me3, mixed-lineage leukemia 1 (MLL1), and H3K4Me3 were detected by western blotting with the corresponding antibodies. As indicated, TBP serves as the loading control. (b,c) The nuclear locations of (b) EZH2 and (c) MLL1 were determined by confocal microscopy after Alexa488-labeling (green) with the corresponding antibodies and staining with DAPI (blue). (d,e) ChIP assays using antibodies against (d) EZH2 and (e) MLL1 were performed and analyzed by qPCR. MLL1 siRNA was transfected into cells and incubated for 24 h. (f) Nuclear fractions were electrophoresed, and MLL1 was detected by western blotting with the corresponding antibodies. As indicated, TBP serves as the loading control. mRNA levels of MLL1 and p16^{INK4A} were detected by qRT-PCR. * $p < 0.05$ and ** $p < 0.05$ indicate significant differences with control cells and PM_{2.5}-treated cells, respectively.

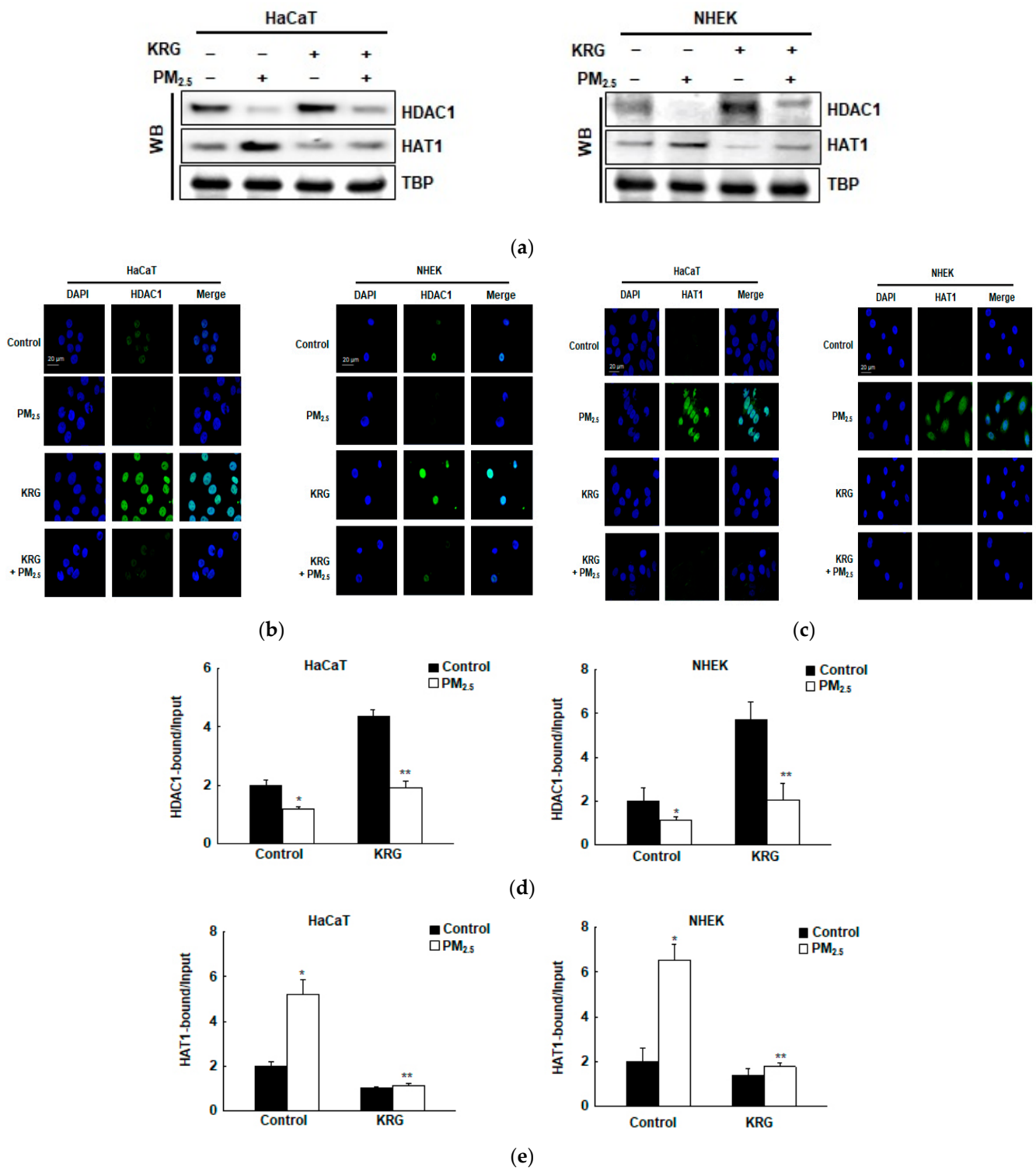


Figure 5. Cont.

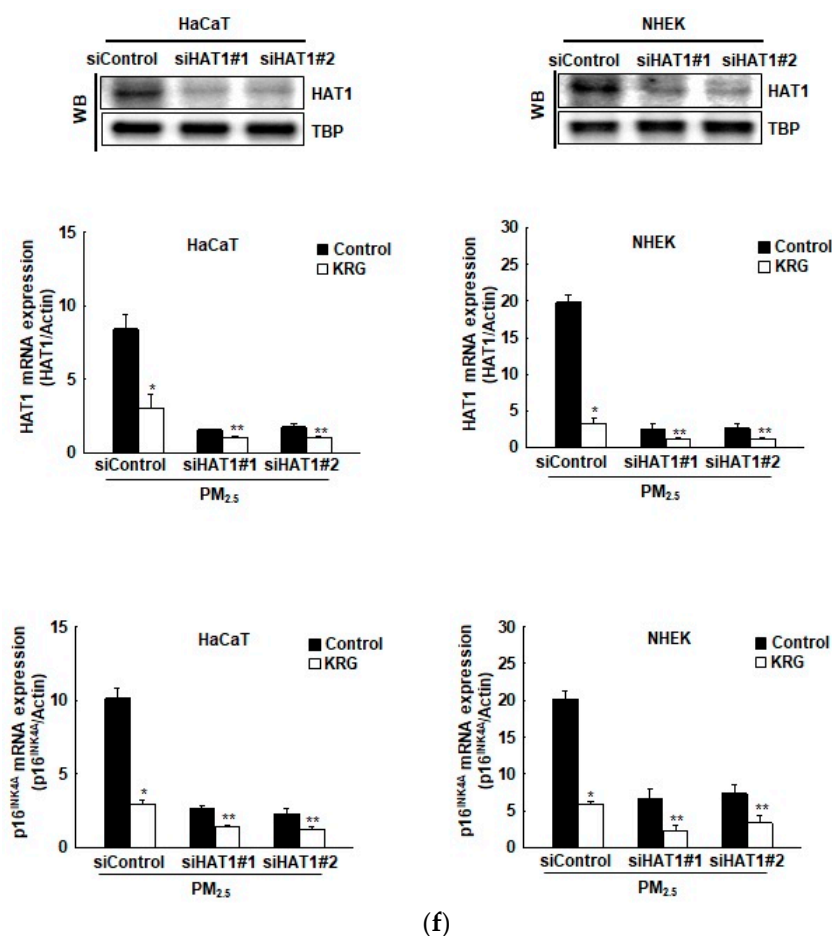


Figure 5. Attenuation of p16^{INK4A} expression in KRG-treated cells via changes in histone acetylation and deacetylation. (a) Nuclear fractions were electrophoresed, and histone deacetyltransferase 1 (HDAC1) and histone acetyltransferase 1 (HAT1) were detected using western blotting with the corresponding antibodies. As indicated, TBP serves as the loading control. (b,c) The nuclear locations of (b) HDAC1 and (c) HAT1 were determined by confocal microscopy after Alexa488-labeling (green) with the corresponding antibodies and staining with DAPI (blue). (d,e) ChIP assays using antibodies against (d) HDAC1 and (e) HAT1 were performed and analyzed by qPCR. HAT1 siRNA was transfected into cells and incubated for 24 h. (f) Nuclear fractions were electrophoresed, and HAT1 was detected using western blotting with the corresponding antibodies. As indicated, TBP serves as the loading control. The mRNA levels of HAT1 and p16^{INK4A} were detected by qRT-PCR. * $p < 0.05$ and ** $p < 0.01$ indicate significant differences with control cells and PM_{2.5}-treated cells, respectively.

4. Discussion

PM_{2.5} has been reported to cause skin diseases such as allergies, inflammatory dermatitis, and skin senescence, resulting in harmful effects on the skin. We have previously reported that PM_{2.5} induced an increase in oxidative stress through the aryl hydrocarbon receptor-ROS pathway and promoted the binding of TET1 and MLL1, instead of DNMT1 and EZH2, to the p16^{INK4A} promoter region. This binding induced the expression of p16^{INK4A}, ultimately inducing human epidermal keratinocytes senescence [9].

KRG has been reported to have more pharmacological efficacy than that of fresh and white ginseng [37]. About 40 types of ginsenosides, including Rb1, Rb2, Rc, Rd, Re, and Rg1 as main bioactive ingredients, have been identified in KRG [37,38]. All compounds exhibit their own biological activity, such as anticancer, anti-inflammatory, antioxidant, antibacterial, antiviral, and antifungal effects, but when mixed or combined, they can produce additive, synergistic, or increased effects [38–42].

Many studies have been conducted on the pharmacological properties of KRG with regard to skin senescence [43–45]. KRG has been shown to prevent endothelial senescence by downregulating the NF- κ B/miRNA-155-5p/eNOS pathway [43]. In addition, the enzyme-modified ginseng extract from KRG has shown protective effects against ultraviolet-B-induced skin senescence in human skin fibroblasts [46]. Furthermore, several studies have explored the anti-senescence effects of ginsenosides, the main component of KRG [47–50]. For instance, ginsenoside Rb1 alleviates oxidative low-density lipoprotein-induced vascular endothelium senescence via the SIRT1/beclin-1/autophagy axis [47]. Additionally, ginsenoside Rg3 inhibits the senescence of prostate stromal cells through the down-regulation of interleukin 8 expression [48].

However, total extracts of ginseng are more beneficial and effective than single ginsenosides or combinations of specific ginsenosides [42]. Here, we determined the anti-senescent efficacy of KRG and the underlying molecular mechanism involving the epigenetic regulation of p16^{INK4A}, a senescence sensor, in PM_{2.5}-induced senescence. Our results have shown that KRG decreases the cellular senescence phenotypes associated with PM_{2.5}-induced oxidative stress, including flattened and enlarged cell shapes, SAHF-like chromatin foci, and β -galactosidase activity in skin keratinocytes.

As a CDK4/CDK6 inhibitor, p16^{INK4A} plays a vital role in senescence formation. The p16^{INK4A} protein is relatively stable, and its expression is mainly controlled at the transcriptional level. Abnormal p16^{INK4A} hypermethylation is found in most tumors and reduces gene expression [51–53]. In mammalian cells, DNMTs maintain global and gene-specific de novo DNA methylation [24]. TETs have the ability to reverse this methylation process. When cells were exposed to PM_{2.5} in this study, TET1 replaced DNMT1 in the p16^{INK4A} promoter region, promoting p16^{INK4A} transcription. KRG pre-treatment in the cells that were treated with PM_{2.5} reversed the altered expressions of DNMTs and TETs. In addition, KRG decreased TET1 binding to the p16^{INK4A} locus and increased DNMT1 binding, thereby reversing the increase in p16^{INK4A} expression and preventing cellular senescence.

Histone methylation via EZH2 and MLL1 is also vital for gene transcription. A methyltransferase EZH2 binds to the p16^{INK4A} locus, inhibiting p16^{INK4A} transcription. Conversely, the p16^{INK4A} locus binding of MLL1 induces transcription during replication and premature senescence [54,55]. In the presence of PM_{2.5}, MLL1 replaced EZH2 in the skin keratinocytes, thereby promoting the transcription of p16^{INK4A}. However, KRG suppressed this effect. In addition to EZH2 and MLL1, the modification of histone acetylation via HAT or HDAC plays an important role in gene transcription [25,56]. In our study, PM_{2.5} induced p16^{INK4A} expression via histone acetylation with HAT1. However, KRG reversed p16^{INK4A} expression via histone deacetylation with HDAC1.

Considering these results, we conclude that p16^{INK4A} expression induced by PM_{2.5} is suppressed by KRG via the epigenetic regulation of DNA and histones, which results in the inhibition of cellular senescence. As KRG inhibited the p16^{INK4A} expression induced by PM_{2.5} through epigenetic regulation, it can be inferred that KRG protects the skin against PM_{2.5} exposure and reduces skin senescence. However, it remains unclear how other epigenetic regulation processes, such as those involving microRNA, are regulated during cellular senescence induced by PM_{2.5}, and how KRG executes epigenetic regulation process of microRNA modulated by PM_{2.5}. Hence, further studies are needed in order to determine other epigenetic regulation processes affecting cellular senescence.

Author Contributions: Experimental design, K.A.K., J.M.Y. and J.W.H.; Data collection, K.A.K., M.J.P. and P.D.S.M.F.; Formal analysis, K.A.K. and H.M.U.L.H.; Writing and supervision, K.A.K., M.J.P. and J.W.H., K.A.K. and M.J.P. contributed equally to this work. All authors have read and agreed to the published version of the manuscript.

Funding: This work was supported by a 2019 grant from the Korean Society of Ginseng.

Institutional Review Board Statement: Not applicable.

Informed Consent Statement: Not applicable.

Data Availability Statement: The data presented in this study are available within this manuscript.

Conflicts of Interest: The authors declare no conflict of interest.

References

1. Son, J.Y.; Lee, J.T.; Kim, K.H.; Jung, K.; Bell, M.L. Characterization of fine particulate matter and associations between particulate chemical constituents and mortality in Seoul, Korea. *Environ. Health Perspect.* **2012**, *120*, 872–878. [[CrossRef](#)]
2. Yuan, Q.; Chen, Y.; Li, X.; Zhang, Z.; Chu, H. Ambient fine particulate matter (PM_{2.5}) induces oxidative stress and pro-inflammatory response via up-regulating the expression of CYP1A1/1B1 in human bronchial epithelial cells in vitro. *Mutat. Res.* **2019**, *839*, 40–48. [[CrossRef](#)]
3. Cao, J.; Qin, G.; Shi, R.; Bai, F.; Yang, G.; Zhang, M.; Lv, J. Overproduction of reactive oxygen species and activation of MAPKs are involved in apoptosis induced by PM_{2.5} in rat cardiac H9c2 cells. *J. Appl. Toxicol.* **2016**, *36*, 609–617. [[CrossRef](#)] [[PubMed](#)]
4. Wang, Y.; Xiong, L.; Tang, M. Toxicity of inhaled particulate matter on the central nervous system: Neuroinflammation, neuropsychological effects and neurodegenerative disease. *J. Appl. Toxicol.* **2017**, *37*, 644–667. [[CrossRef](#)]
5. Li, N.; He, F.; Liao, B.; Zhou, Y.; Li, B.; Ran, P. Exposure to ambient particulate matter alters the microbial composition and induces immune changes in rat lung. *Respir. Res.* **2017**, *18*, 143. [[CrossRef](#)] [[PubMed](#)]
6. Pan, T.L.; Wang, P.W.; Aljuffali, I.A.; Huang, C.T.; Lee, C.W.; Fang, J.Y. The impact of urban particulate pollution on skin barrier function and the subsequent drug absorption. *J. Dermatol. Sci.* **2015**, *78*, 51–60. [[CrossRef](#)]
7. Kim, K.E.; Cho, D.; Park, H.J. Air pollution and skin diseases: Adverse effects of airborne particulate matter on various skin diseases. *Life Sci.* **2016**, *152*, 126–134. [[CrossRef](#)]
8. Magnani, N.D.; Muresan, X.M.; Belmonte, G.; Cervellati, F.; Sticozzi, C.; Pecorelli, A.; Miracco, C.; Marchini, T.; Evelson, P.; Valacchi, G. Skin damage mechanisms related to airborne particulate matter exposure. *Toxicol. Sci.* **2016**, *149*, 227–236. [[CrossRef](#)] [[PubMed](#)]
9. Ryu, Y.S.; Kang, K.A.; Piao, M.J.; Ahn, M.J.; Yi, J.M.; Bossis, G.; Hyun, Y.M.; Park, C.O.; Hyun, J.W. Particulate matter-induced senescence of skin keratinocytes involves oxidative stress-dependent epigenetic modifications. *Exp. Mol. Med.* **2019**, *51*, 1–14. [[CrossRef](#)] [[PubMed](#)]
10. Rider, C.F.; Carlsten, C. Air pollution and DNA methylation: Effects of exposure in humans. *Clin. Epigenetics.* **2019**, *11*, 131. [[CrossRef](#)]
11. Pulliero, A.; Traversi, D.; Franchitti, E.; Barchitta, M.; Izzotti, A.; Agodi, A. The interaction among microbiota, epigenetic regulation, and air pollutants in disease prevention. *J. Pers. Med.* **2021**, *12*, 14. [[CrossRef](#)] [[PubMed](#)]
12. Ito, S.; Shen, L.; Dai, Q.; Wu, S.C.; Collins, L.B.; Swenberg, J.A.; He, C.; Zhang, Y. Tet proteins can convert 5-methylcytosine to 5-formylcytosine and 5-carboxylcytosine. *Science* **2011**, *333*, 1300–1303. [[CrossRef](#)]
13. Oh, J.H.; Jung, S.H.; Hong, S.J.; Rhyu, M.G. DNA methylation as surrogate marker for gastric cancer. *J. Cancer Prev.* **2015**, *20*, 172–178. [[CrossRef](#)]
14. Bannister, A.J.; Kouzarides, T. Regulation of chromatin by histone modifications. *Cell Res.* **2011**, *21*, 381–395. [[CrossRef](#)]
15. Jambhekar, A.; Dhall, A.; Shi, Y. Roles and regulation of histone methylation in animal development. *Nat. Rev. Mol. Cell Biol.* **2019**, *20*, 625–641. [[CrossRef](#)] [[PubMed](#)]
16. Zhao, L.; Zhang, Y.; Gao, Y.; Geng, P.; Lu, Y.; Liu, X.; Yao, R.; Hou, P.; Liu, D.; Lu, J.; et al. JMJD3 promotes SAHF formation in senescent WI38 cells by triggering an interplay between demethylation and phosphorylation of RB protein. *Cell Death Differ.* **2015**, *22*, 1630–1640. [[CrossRef](#)] [[PubMed](#)]
17. He, S.; Sharpless, N.E. Senescence in health and disease. *Cell* **2017**, *169*, 1000–1011. [[CrossRef](#)]
18. Crouch, J.; Shvedova, M.; Thanapaul, R.J.R.S.; Botchkarev, V.; Roh, D. Epigenetic regulation of cellular senescence. *Cells* **2022**, *11*, 672. [[CrossRef](#)]
19. Zhao, R.; Choi, B.Y.; Lee, M.H.; Bode, A.M.; Dong, Z. Implications of genetic and epigenetic alterations of CDKN2A (p16^{INK4a}) in cancer. *EBioMedicine* **2016**, *8*, 30–39. [[CrossRef](#)]
20. Song, W.; Liu, Y.; Liu, Y.; Zhang, C.; Yuan, B.; Zhang, L.; Sun, S. Increased p16 DNA methylation in mouse thymic lymphoma induced by irradiation. *PLoS ONE* **2014**, *9*, e93850. [[CrossRef](#)]
21. Zhu, B.; Gong, Y.; Yan, G.; Wang, D.; Wang, Q.; Qiao, Y.; Hou, J.; Liu, B.; Tang, C. Atorvastatin treatment modulates p16 promoter methylation to regulate p16 expression. *FEBS J.* **2017**, *284*, 1868–1881. [[CrossRef](#)]
22. D’Arcangelo, D.; Tinaburri, L.; Dellambra, E. The role of p16^{INK4a} pathway in human epidermal stem cell self-renewal, aging and cancer. *Int. J. Mol. Sci.* **2017**, *18*, 1591. [[CrossRef](#)]
23. Zhu, X.; Leboeuf, M.; Liu, F.; Grachtchouk, M.; Seykora, J.T.; Morrisey, E.E.; Dlugosz, A.A.; Millar, S.E. HDAC1/2 control proliferation and survival in adult epidermis and pre-basal cell carcinoma through p16 and p53. *J. Investig. Dermatol.* **2022**, *142*, 77–87. [[CrossRef](#)] [[PubMed](#)]
24. Kotake, Y.; Naemura, M.; Murasaki, C.; Inoue, Y.; Okamoto, H. Transcriptional regulation of the p16 tumor suppressor gene. *Anticancer Res.* **2015**, *35*, 4397–4401. [[PubMed](#)]
25. Wang, W.; Pan, K.; Chen, Y.; Huang, C.; Zhang, X. The acetylation of transcription factor HBP1 by p300/CBP enhances p16^{INK4A} expression. *Nucleic Acids Res.* **2012**, *40*, 981–995. [[CrossRef](#)] [[PubMed](#)]
26. So, S.; Lee, J.W.; Kim, Y.; Hyun, S.H.; Han, C. Red ginseng monograph. *J. Ginseng Res.* **2018**, *42*, 549–561. [[CrossRef](#)]

27. Kim, E.J.; Kwon, K.A.; Lee, Y.E.; Kim, J.H.; Kim, S.H.; Kim, J.H. Korean red ginseng extract reduces hypoxia-induced epithelial-mesenchymal transition by repressing NF- κ B and ERK1/2 pathways in colon cancer. *J. Ginseng Res.* **2018**, *42*, 288–297. [[CrossRef](#)]
28. Sung, W.N.; Kwok, H.H.; Rhee, M.H.; Yue, P.Y.; Wong, R.N. Korean red ginseng extract induces angiogenesis through activation of glucocorticoid receptor. *J. Ginseng Res.* **2017**, *41*, 477–486. [[CrossRef](#)]
29. Kim, Y.M.; Kim, J.H.; Kwon, H.M.; Lee, D.H.; Won, M.H.; Kwon, Y.G.; Kim, Y.M. Korean red ginseng protects endothelial cells from serum-deprived apoptosis by regulating Bcl-2 family protein dynamics and caspase S-nitrosylation. *J. Ginseng Res.* **2013**, *37*, 413–424. [[CrossRef](#)]
30. Yang, H.; Lee, S.E.; Jeong, S.I.; Park, C.S.; Jin, Y.H.; Park, Y.S. Up-regulation of heme oxygenase-1 by Korean red ginseng water extract as a cytoprotective effect in human endothelial cells. *J. Ginseng Res.* **2011**, *35*, 352–359. [[CrossRef](#)]
31. Lee, S.; Park, J.M.; Jeong, M.; Han, Y.M.; Go, E.J.; Ko, W.J.; Cho, J.Y.; Kwon, C.I.; Hahm, K.B. Korean red ginseng ameliorated experimental pancreatitis through the inhibition of hydrogen sulfide in mice. *Pancreatol.* **2016**, *16*, 326–336. [[CrossRef](#)]
32. Schubert, P.; Schantz, M.M.; Sander, L.C.; Wise, S.A. Determination of polycyclic aromatic hydrocarbons with molecular weight 300 and 302 in environmental-matrix standard reference materials by gas chromatography/mass spectrometry. *Anal. Chem.* **2003**, *75*, 234–246. [[CrossRef](#)]
33. Bezabeh, D.Z.; Bamford, H.A.; Schantz, M.M.; Wise, S.A. Determination of nitrated polycyclic aromatic hydrocarbons in diesel particulate-related standard reference materials by using gas chromatography/mass spectrometry with negative ion chemical ionization. *Anal. Bioanal. Chem.* **2003**, *375*, 381–388. [[CrossRef](#)]
34. Piao, M.J.; Ahn, M.J.; Kang, K.A.; Ryu, Y.S.; Hyun, Y.J.; Shilnikova, K.; Zhen, A.X.; Jeong, J.W.; Choi, Y.H.; Kang, H.K.; et al. Particulate matter 2.5 damages skin cells by inducing oxidative stress, subcellular organelle dysfunction, and apoptosis. *Arch. Toxicol.* **2018**, *92*, 2077–2091. [[CrossRef](#)]
35. Herman, J.G.; Graff, J.R.; Myöhänen, S.; Nelkin, B.D.; Baylin, S.B. Methylation-specific PCR: A novel PCR assay for methylation status of CpG islands. *Proc. Natl. Acad. Sci. USA* **1996**, *93*, 9821–9826. [[CrossRef](#)]
36. McGarvey, K.M.; Greene, E.; Fahrner, J.A.; Jenuwein, T.; Baylin, S.B. DNA methylation and complete transcriptional silencing of cancer genes persist after depletion of EZH2. *Cancer Res.* **2007**, *67*, 5097–5102. [[CrossRef](#)]
37. Lee, S.M.; Bae, B.S.; Park, H.W.; Ahn, N.G.; Cho, B.G.; Cho, Y.L.; Kwak, Y.S. Characterization of Korean red ginseng (*Panax ginseng* Meyer): History, preparation method, and chemical composition. *J. Ginseng Res.* **2015**, *39*, 384–391. [[CrossRef](#)]
38. Ratan, Z.A.; Haidere, M.F.; Hong, Y.H.; Park, S.H.; Lee, J.O.; Lee, J.; Cho, J.Y. Pharmacological potential of ginseng and its major component ginsenosides. *J. Ginseng Res.* **2021**, *45*, 199–210. [[CrossRef](#)]
39. Wahid, F.; Khan, T.; Subhan, F.; Khan, M.; Kim, Y. Ginseng pharmacology: Multiple molecular targets and recent clinical trials. *Drugs Future* **2010**, *35*, 399–407. [[CrossRef](#)]
40. Lee, D.; Lee, D.S.; Jung, K.; Hwang, G.S.; Lee, H.L.; Yamabe, N.; Lee, H.J.; Eom, D.W.; Kim, K.H.; Kang, K.S. Protective effect of ginsenoside Rb1 against tacrolimus-induced apoptosis in renal proximal tubular LLC-PK1 cells. *J. Ginseng Res.* **2018**, *42*, 75–80. [[CrossRef](#)]
41. Kim, M.K.; Kang, H.; Baek, C.W.; Jung, Y.H.; Woo, Y.C.; Choi, G.J.; Shin, H.Y.; Kim, K.S. Antinociceptive and anti-inflammatory effects of ginsenoside Rf in a rat model of incisional pain. *J. Ginseng Res.* **2018**, *42*, 183–191. [[CrossRef](#)] [[PubMed](#)]
42. Saw, C.L.; Yang, A.Y.; Cheng, D.C.; Boyanapalli, S.S.; Su, Z.Y.; Khor, T.O.; Gao, S.; Wang, J.; Jiang, Z.H.; Kong, A.N. Pharmacodynamics of ginsenosides: Antioxidant activities, activation of Nrf2, and potential synergistic effects of combinations. *Chem. Res. Toxicol.* **2012**, *25*, 1574–1580. [[CrossRef](#)] [[PubMed](#)]
43. Kim, T.H.; Kim, J.Y.; Bae, J.; Kim, Y.M.; Won, M.H.; Ha, K.S.; Kwon, Y.G.; Kim, Y.M. Korean red ginseng prevents endothelial senescence by downregulating the HO-1/NF- κ B/miRNA-155-5p/eNOS pathway. *J. Ginseng Res.* **2021**, *45*, 344–353. [[CrossRef](#)] [[PubMed](#)]
44. Cho, E.G.; Choi, S.Y.; Kim, H.; Choi, E.J.; Lee, E.J.; Park, P.J.; Ko, J.; Kim, K.P.; Baek, H.S. Panax ginseng-derived extracellular vesicles facilitate anti-senescence effects in human skin cells: An eco-friendly and sustainable way to use ginseng substances. *Cells* **2021**, *10*, 486. [[CrossRef](#)]
45. Chung, T.H.; Kim, J.H.; Seol, S.Y.; Kim, Y.J.; Lee, Y.J. The effects of Korean red ginseng on biological aging and antioxidant capacity in postmenopausal women: A double-blind randomized controlled study. *Nutrients* **2021**, *13*, 3090. [[CrossRef](#)]
46. Hwang, E.; Lee, T.H.; Park, S.Y.; Yi, T.H.; Kim, S.Y. Enzyme-modified Panax ginseng inhibits UVB-induced skin aging through the regulation of procollagen type I and MMP-1 expression. *Food Funct.* **2014**, *5*, 265–274. [[CrossRef](#)]
47. Shi, G.; Liu, D.; Zhou, B.; Liu, Y.; Hao, B.; Yu, S.; Wu, L.; Wang, M.; Song, Z.; Wu, C.; et al. Ginsenoside Rb1 alleviates oxidative low-density lipoprotein-induced vascular endothelium senescence via the SIRT1/beclin-1/autophagy axis. *J. Cardiovasc. Pharmacol.* **2020**, *75*, 155–167. [[CrossRef](#)]
48. Peng, Y.; Zhang, R.; Kong, L.; Shen, Y.; Xu, D.; Zheng, F.; Liu, J.; Wu, Q.; Jia, B.; Zhang, J. Ginsenoside Rg3 inhibits the senescence of prostate stromal cells through down-regulation of interleukin 8 expression. *Oncotarget* **2017**, *8*, 64779–64792. [[CrossRef](#)]
49. Wang, Z.; Wang, L.; Jiang, R.; Li, C.; Chen, X.; Xiao, H.; Hou, J.; Hu, L.; Huang, C.; Wang, Y. Ginsenoside Rg1 prevents bone marrow mesenchymal stem cell senescence via NRF2 and PI3K/Akt signaling. *Free Radic. Biol. Med.* **2021**, *174*, 182–194. [[CrossRef](#)]
50. Chen, Y.; Wang, S.; Yang, S.; Li, R.; Yang, Y.; Chen, Y.; Zhang, W. Inhibitory role of ginsenoside Rb2 in endothelial senescence and inflammation mediated by microRNA-216a. *Mol. Med. Rep.* **2021**, *23*, 415. [[CrossRef](#)]
51. Kia, S.K.; Gorski, M.M.; Giannakopoulos, S.; Verrijzer, C.P. SWI/SNF mediates polycomb eviction and epigenetic reprogramming of the INK4b-ARF-INK4a locus. *Mol. Cell Biol.* **2008**, *28*, 3457–3464. [[CrossRef](#)] [[PubMed](#)]

52. Nikolic, N.; Anicic, B.; Carkic, J.; Simonovic, J.; Toljic, B.; Tanic, N.; Tepavcevic, Z.; Vukadinovic, M.; Konstantinovic, V.S.; Milasin, J. High frequency of p16 and p14 promoter hypermethylation and marked telomere instability in salivary gland tumors. *Arch. Oral. Biol.* **2015**, *60*, 1662–1666. [[CrossRef](#)]
53. Zhou, W.; Tian, D.; He, J.; Wang, Y.; Zhang, L.; Cui, L.; Jia, L.; Zhang, L.; Li, L.; Shu, Y.; et al. Repeated PM_{2.5} exposure inhibits BEAS-2B cell p53 expression through ROS-Akt-DNMT3B pathway-mediated promoter hypermethylation. *Oncotarget* **2016**, *7*, 20691–20703. [[CrossRef](#)] [[PubMed](#)]
54. Kang, K.A.; Piao, M.J.; Ryu, Y.S.; Kang, H.K.; Chang, W.Y.; Keum, Y.S.; Hyun, J.W. Interaction of DNA demethylase and histone methyltransferase upregulates Nrf2 in 5-fluorouracil-resistant colon cancer cells. *Oncotarget* **2016**, *7*, 40594–40620. [[CrossRef](#)]
55. Gonçalves, A.C.; Cortesão, E.; Oliveiros, B.; Alves, V.; Espadana, A.I.; Rito, L.; Magalhães, E.; Pereira, S.; Pereira, A.; Costa, J.M.; et al. Oxidative stress levels are correlated with p15 and p16 gene promoter methylation in myelodysplastic syndrome patients. *Clin. Exp. Med.* **2016**, *16*, 333–343. [[CrossRef](#)] [[PubMed](#)]
56. Liu, Z.; Lin, H.; Gan, Y.; Cui, C.; Zhang, B.; Gu, L.; Zhou, J.; Zhu, G.; Deng, D. p16 methylation leads to paclitaxel resistance of advanced non-small cell lung cancer. *J. Cancer* **2019**, *10*, 1726–1733. [[CrossRef](#)]

Disclaimer/Publisher’s Note: The statements, opinions and data contained in all publications are solely those of the individual author(s) and contributor(s) and not of MDPI and/or the editor(s). MDPI and/or the editor(s) disclaim responsibility for any injury to people or property resulting from any ideas, methods, instructions or products referred to in the content.